Engineering Structures 128 (2016) 474–487

Contents lists available at ScienceDirect

Engineering Structures

journal homepage: www.elsevier.com/locate/engstruct

Buffeting response of a suspension bridge in complex terrain

Etienne Cheynet [a,*], Jasna Bogunović Jakobsen [a], Jónas Snæbjörnsson [a,b]

[a] Department of Mechanical and Structural Engineering and Materials Science, University of Stavanger, N-4036 Stavanger, Norway
[b] School of Science and Engineering, Reykjavik University, Menntavegur 1, 101 Reykjavk, Iceland

ARTICLE INFO

Article history:
Received 30 October 2015
Revised 24 June 2016
Accepted 27 September 2016

Keywords:
Full-scale measurement
Long-span bridge
Complex topography
Turbulence
Wind excitation
Buffeting response
Frequency domain

ABSTRACT

The buffeting response of a suspension bridge in complex terrain is studied based on full-scale data from sonic anemometers and accelerometers installed on the Lysefjord Bridge in Norway. The influence of the topography on the wind field and the associated effects on the displacement response are investigated. The two main wind conditions observed display different characteristics, which requires a case by case approach, and a refined description of the wind co-coherence. The identification of the mode shapes and modal damping ratios is carried out using ambient vibration data as a verification procedure. The buffeting response of the bridge is computed in the frequency domain, and compared to the recorded response in terms of standard deviation and power spectral density of the displacement response. The overall comparison is found satisfactory, although some discrepancies are observed. These are attributed to large yaw angles and non-stationary wind fluctuations caused by the influence of a complex topography on the flow properties.

1. Introduction

The buffeting theory, introduced more than 50 years ago by Davenport [1] and developed by e.g. Scanlan [2] is the standard approach for calculating the response of a suspension bridge to wind turbulence. The development of advanced Wind And Structural Health Monitoring (WASHM) systems at the end of the 1990's [3] has given the opportunity to assess the validity of the buffeting theory in full scale. Unfortunately, studies dealing with this subject remain a rarity. This is mostly because they require resources and a cross-disciplinary knowledge to fullfil three criteria: The identification of the modal parameters of the bridge, the measurements of its response, and the measurements of the single and two-point statistics of wind turbulence. Apart from Bietry et al. [4], no WASHM systems-based studies currently addresses these three aspects (Table 1). The meticulous full-scale analysis of Xu et al. [5] and Macdonald [6] did not capture the wind coherence. On the other hand, cases containing detailed measurements of the wind-field [7–9] were not accompanied by bridge vibrations analysis. Toriumi et al. [10] or Miyata et al. [11] are among those who simultaneously studied full scale wind-induced vibrations and two-point statistics of wind turbulence. Unfortunately, none of them appears to have carried out a modal-identification (MI) procedure. The limiting factor in the works of Bietry et al. [4] was that the duration of the data analyzed was limited to 6 h, which is too short to assess the validity of the buffeting theory in full-scale. Consequently, the statistical significance achieved by considering wind and acceleration data with a duration large enough can constitute a fourth criteria to be fullfilled to verify the buffeting theory. Analysis of bridge response to Typhoon wind [11,10,5] may therefore fail the fourth criteria because of the short duration of the measurement period. In summary, there is an anomaly in the field of wind engineering, where suspension bridges are designed based on a theory that has never been thoroughly verified in full scale.

We present herein results from a full-scale buffeting analysis of a suspension bridge that fullfils the four criteria previously mentioned, by the means of simultaneous full-scale recordings of wind velocity and acceleration response from sensors installed directly on and inside the bridge deck. We also aim to synthesize results from previous studies to lay the foundations of a rigorous buffeting analysis of suspension bridges in full-scale. The uniqueness of the present work is emphasized by the geographical location of the bridge studied, which is built between two cliffs in a mountainous environment in Norway. Analysis of bridge response to Typhoon winds [10,11,5] have limited relevance in Western Europe, where the design wind conditions are generally caused by subtropical cyclones stemming from severe winter lows from the North Atlantic ocean. Similar studies of their European counterparts are therefore necessary for future ultra-long span suspension bridges.

In the present paper, an operational modal analysis is first conducted based on the wind and acceleration data provided during the period of study. It is followed by an analysis of the statistics

* Corresponding author.
E-mail address: etienne.cheynet@uis.no (E. Cheynet).

http://dx.doi.org/10.1016/j.engstruct.2016.09.060
0141-0296/

Table 1
Review of wind and bridge vibrations monitoring at full scale (done: +; not done: –).

Reference	MI	Buffeting response		Wind statistic	
		Computed	Measured	1-point	2-points
Present work	+	+	+	+	+
Bietry et al. [4]	+	+	+	+	+
Miyata et al. [11]	–	–	+	+	+
Toriumi et al. [10]	–	–	+	+	+
Wang et al. [12]	–	–	–	+	+
Hui et al. [8,7]	–	–	–	+	+
Wang et al. [9]	–	+	+	+	–
Xu et al. [5]	+	+	+	+	–
Macdonald [6]	+	+	+	+	–
Nakamura [13]	+	–	–	+	–
Brownjohn et al. [14]	+	–	+	+	–
Nagayama et al. [15]	+	–	+	–	–
Hay [16]	–	–	+	–	–

of wind turbulence, and a comparison between the measured and computed buffeting response of the suspension bridge used for the case study. The focus of the discussion will be on the influence of the topography on the flow conditions, as well on the limits of the numerical model used.

2. The bridge site and instrumentation

The Lysefjord Bridge, located at the narrow inlet of a Norwegian fjord, is used as a study case. It is oriented from North-West to South-East in a mountainous environment. It is entrenched between two steep hills with slopes ranging from 30° to 45° and a maximum altitude of 350 m to the North and 600 m to the South. Its East side is exposed to winds that may descent from mountains nearby or follow the fjord over a longer path. The west side of the bridge is exposed to a more open and leveled area, where the wind may be accelerated in the vicinity of the bridge because of the narrowing effect of the fjord (Fig. 1). Influence of complex terrain on the wind field properties was observed by Hui et al. [7,8] and studied by Frank [17] and Mann [18] but without evaluating the consequences for wind-sensitive civil structures. Consequently, we study herein the bridge response to wind turbulence using a case-by-case approach, where the wind from the East side of the bridge is studied separately from the wind from the West side.

The anemometers are installed on the West side of the bridge on hangers No. 8, 10, 16, 18, 20 and 24, as indicated in Fig. 2. There is one anemometer per hanger except on hanger No. 8 (H-08), where two of them are mounted at 6 m (H-08b) and 10 m (H-08t) above the bridge deck. The other anemometers are placed about 6 m above the deck, and the distance between hangers is 12 m. The instruments used are 3D WindMaster Pro sonic anemometers from Gill Instrument Ltd, except the one installed on hanger 10, which is a Vaisala weather transmitter WXT520. Four couples of tri-axial accelerometers are located inside the bridge deck, near hangers 9, 18, 24, and 30. The accelerometers are placed on each side of the deck to monitor the bridge torsional motion around its longitudinal axis (y), in addition to the translational response. GPS timing is used to synchronize the data, and a 3G router enables wireless data access and transfer via a mobile net. The data is initially sampled at 100 Hz and registered on an online server. The dynamic displacement of the bridge is obtained based on the acceleration data through Fourier transform multiplication. Considering the frequency range of interest, the sampling frequency is reduced to 20 Hz for lighter data processing.

The wind-based coordinate system shown in Fig. 2, defines three orthogonal wind speed components. The first one is desig-

Fig. 1. View to the North-East (top left), to the South-West (bottom-left) and view of the bridge (right).

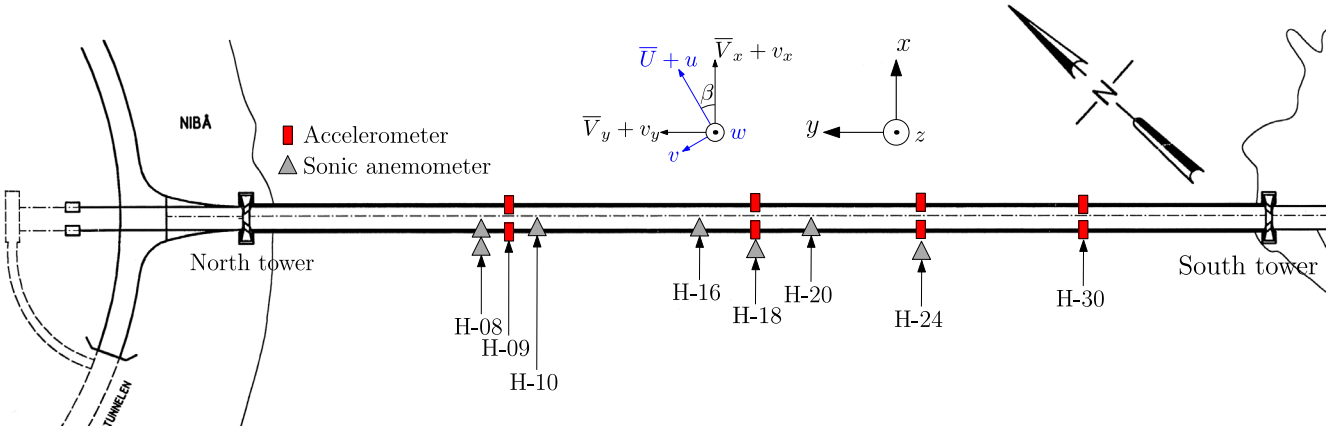

Fig. 2. Anemometers (triangles) and accelerometers (rectangles) location on the bridge.

nated by $\overline{U}+u$ where $\overline{U}$ is the horizontal mean wind speed and u is its turbulent component. The two other components are v and $\overline{W}+w$. The vertical mean wind velocity $\overline{W}$ is here assumed zero for simplicity, even though that is usually not the case. To take into account the effects of the wind directionality on structural response, the wind components are expressed in the coordinate system of the bridge. The angle between the wind direction and the normal to the bridge, also called yaw angle, is denoted β. The wind velocity components in this reference system are $\overline{V}_x+v_x, \overline{V}_y+v_y$, and w. The bridge-based coordinate system defined here is equivalent to the "cosine rule" previously used to study the effects of skew winds on structures [19–21]. The main difference lies on the introduction of the yaw angle directly into the time histories of the wind records instead of into their respective power spectral densities and coherence functions, which is more convenient for a full-scale analysis.

3. Modal parameters identification

An automated covariance driven stochastic subspace identification method (SSI-COV) entirely inspired from the one developed by Magalhães et al. [22,23] is used in the present study. Brownjohn et al. [24] showed that this method has good accuracy compared to the ERA [25] and p-LSCF algorithm [26]. We expand the analysis of Brownjohn et al. [24] by applying for the first time this automated SSI-COV method to estimate the evolution of the aerodynamic modal damping ratio with the mean wind velocity. In the case of Lysefjord Bridge, the structural modal damping ratios are expected to be lower than 1%, as is typical in suspension bridges with steel welded box-girders. The first goal of the present modal analysis is to compare the measured eigen-frequencies and mode shapes with those provided by the Finite Element-based software ALVSAT used by the Norwegian Public Road Administration (NPRA). The second one is to evaluate the suitability of the quasi-steady aerodynamic damping model with the one measured in the present work. The accuracy threshold for the eigen-frequencies, modal damping ratios, the modal assurance criterion (MAC) and the cluster algorithm are denoted ϵ_{fn}, ϵ_{ζ}, ϵ_{MAC} and ϵ_{clus} respectively. The values used in the present study are summarized in Table 2, and compared to the values used by Magalhães et al. [22].

4. Turbulence statistics

In the present study, wind turbulence statistics are calculated in the bridge-based coordinate system, and used directly to estimate the buffeting load. This is equivalent to applying the "cosine rule" to account for the yaw angle effect, but more straightforward. For the single-point statistics, results are also presented in the wind-based coordinate system, to provide data comparable to those in the literature. This applies to the wind spectra, the integral length scales and the turbulence intensity. This is for example pertinent for assessing the applicability of the von Kármán spectrum in fjords. A detailed analysis of turbulence statistics is outside the scope of the present study and requires analysis of a larger data set. Therefore, we summarize in the following only the most relevant turbulence statistics for the buffeting analysis of the Lysefjord Bridge.

Table 2
Accuracy test thresholds used with the automated SSI-COV procedure.

Threshold parameter	Ref. [22]	Present study
ϵ_{fn}	0.01	0.01
ϵ_{ζ}	0.02	0.02
ϵ_{MAC}	0.01	0.005
ϵ_{clus}	0.02	0.02

4.1. Single-point statistics

During a full day of observation, 144 samples of 10 min are recorded. The wind spectra are calculated in the wind-based coordinate system for every sample, then normalized. For each component, an average spectrum is calculated as the average of every 10 min spectrum, and displayed as a function of the wave number k, defined as:

$$k=\frac{2\pi f}{\overline{U}} \tag{1}$$

The measured spectrum is then compared to the von Kármán spectrum, the analytic expression of which is taken from Morfiadakis et al. [27]. This requires the calculation of the along-wind turbulence length scales L_u and L_w, calculated as:

$$L_j=\bar{U}\int_{\tau=0}^{\tau\left(R_{jj}(\tau)=0\right)}R_{jj}(\tau)\,\mathrm{d}\tau \tag{2}$$

where $j=\{u,w\}$ and $R_{jj}(\tau)$ is the autocorrelation coefficient function for the fluctuating component j:

$$R_{jj}(\tau)=\frac{E[j(t)j(t+\tau)]}{\sigma_j^2} \tag{3}$$

4.2. Two-point statistics

In the present study, the two-point statistics of wind turbulence is presented through a co-coherence function and is defined as the real part of the normalized cross-spectrum of wind fluctuations [28–30]. The co-coherence takes into account the simultaneous appearance of wind fluctuations along the bridge deck. It is a function of both frequency f and spatial separation. The latter is reduced to a horizontal line for the suspension bridge deck studied, with a resolution fixed by the separation of the individual anemometers, and is therefore denoted d_y. An analytic function represented by a four-parameter exponential decay function is fitted in the least-square sense to the measured co-coherence:

$$\gamma(d_y,f)=exp\left(-\left[\frac{d_y}{\overline{V}_x}\sqrt{(c_1 f)^2+c_2^2}\right]^{c_3}\right)\cdot\cos\left(c_4\frac{d_y f}{\overline{V}_x}\right) \tag{4}$$

The first parameter c_1 gives the slope of the exponential decay, the second one c_2 allows the co-coherence to be lower than one for a zero frequency. The third one c_3 allows an additional inflection point at low frequencies, and the last one c_4 allows the co-coherence to become negative when the frequency increases. When $c_4=0$, the coherence function developed by Bogunović Jakobsen [31] is retrieved. If $c_4=0$ and $c_3=1$, the 2-parameter function introduced by Hjorth-Hansen et al. [32] is obtained. Finally, if $c_4=0$, $c_3=1$ and $c_2=0$, then Eq. (4) reduces to the simple exponential decay model from Davenport [29]. This is the first time that a co-coherence functional form of this type is used to estimate the wind coherence. The goal is to provide a larger flexibility to capture in details the different features of the co-coherence. To investigate the versatility of this 4-parameter function, we successfully fitted it to more complex coherence models such as the one developed by Krenk [33] or von Kármán [34].

As previously stated, this four-parameter exponential decay function could be fitted to the measured co-coherence function for the along and across-wind component to investigate the spatial structure of wind turbulence in complex terrain, but this is out of the scope of the present study.

5. Buffeting analysis

The basic theory to calculate the buffeting response of a suspension bridge in the frequency domain is recalled here, based on the work of Scanlan [2]. The bridge is modeled as a 3-DOF continuous linear damped system (Fig. 3), where the lateral, vertical and torsional motions are taken into account. The aerodynamic derivatives measured in wind tunnel tests were not available for the Lysefjord Bridge, and consequently, only the static aerodynamic coefficients are used in the present study (Table 3). A damping term $k_\theta B\dot{r}_\theta$ for the torsional degree of freedom of a bridge deck was introduced by Irwin et al. [35], where k_θ specifies the horizontal distance between the aerodynamic and the shear center as a fraction of the girder width. In the present study, a value of $k_\theta = 0.25$, representative for the "flat plate like" cross-section, is chosen.

The lateral and vertical displacement and the rotational angle of the deck are denoted r_y, r_z, and r_θ respectively. The aerodynamic drag F_D, lift F_L, and pitching moment F_M are transformed into the lateral wind load F_x, the vertical load F_z and the pitching moment F_θ using a projection at an angle α of the coordinate system on Fig. 3. The dynamic equilibrium leads to the expression of the matrices of buffeting load $\boldsymbol{A}$, aerodynamic damping $\boldsymbol{C}_{ae}$, and stiffness $\boldsymbol{K}_{ae}$ presented in Eqs. (5)–(7), where $\chi_{pq}, p = \{u, w\}$ and $q = \{x, z, \theta\}$ are the cross-sectional aerodynamic admittance functions.

$$\boldsymbol{A} = \frac{1}{2}\rho\overline{V}_x B\begin{bmatrix} 2\frac{D}{B}C_D\cdot\chi_{ux} & \frac{D}{B}C'_D - C_L\cdot\chi_{wx} \\ 2C_L\cdot\chi_{uz} & C'_L + \frac{D}{B}C_D\cdot\chi_{wz} \\ 2BC_M\cdot\chi_{u\theta} & BC'_M\cdot\chi_{w\theta}\end{bmatrix} \tag{5}$$

$$\boldsymbol{C}_{ae} = \frac{1}{2}\rho\overline{V}_x B\begin{bmatrix} 2\frac{D}{B}C_D & \frac{D}{B}C'_D - C_L & k_\theta B(\frac{D}{B}C'_D - C_L) \\ 2C_L & C'_L + \frac{D}{B}C_D & k_\theta B(C'_L + \frac{D}{B}C_D) \\ 2BC_M & BC'_M & k_\theta B^2 C'_M\end{bmatrix} \tag{6}$$

$$\boldsymbol{K}_{ae} = -\frac{1}{2}\rho\overline{V}_x^2 B\begin{bmatrix} 0 & 0 & \frac{D}{B}C'_D \\ 0 & 0 & C'_L \\ 0 & 0 & BC'_M\end{bmatrix} \tag{7}$$

If modal coupling is neglected, the matrices $\boldsymbol{C}_{ae}$ and $\boldsymbol{K}_{ae}$ become diagonal. The real part of the cross-spectral density of the wind velocity between two points of abscissa y_i and y_j is defined using the single-point wind spectra $\boldsymbol{S}_{v_x}$ and $\boldsymbol{S}_w$, and the co-coherence functions γ_{v_x},γ_w:

$$S_1(y_i, y_j, f) = \sqrt{S_{v_x}(y_i, f)\cdot S_{v_x}(y_j, f)}\cdot\gamma_{v_x}(y_i, y_j, f) \tag{8}$$

$$S_2(y_i, y_j, f) = \sqrt{S_w(y_i, f)\cdot S_w(y_j, f)}\cdot\gamma_w(y_i, y_j, f) \tag{9}$$

Table 3
Key structural parameters of the Lysefjord Bridge.

Structural parameters	Symbols	Value
Main span length (m)	L	446
Girder mass (kg/m)	m_g	5350
Main cables mass (kg/m)	m_c	408
Mass moment of inertia (kg m^2/m)	I_θ	82,430
Girder height (m)	D	2.76
Girder width (m)	B	12.3
Drag coefficient	C_D	1.0
Lift coefficient	C_L	0.1
Pitching moment	C_M	0.02
$\frac{\partial C_D}{\partial\alpha}$	C'_D	0.0
$\frac{\partial C_L}{\partial\alpha}$	C'_L	3.0
$\frac{\partial C_M}{\partial\alpha}$	C'_M	1.12

Thus the cross-spectrum matrix $\boldsymbol{S}_{qq}$ of the wind velocities weighted by the matrix of buffeting load coefficients is a block matrix, whose block (i,j) is a 3 by 3 matrix defined as:

$$S_{qq}(i,j,f) = \boldsymbol{A}\begin{bmatrix} S_1(y_i, y_j, f) & 0 \\ 0 & S_2(y_i, y_j, f)\end{bmatrix}\boldsymbol{A}^{\mathrm{T}} \tag{10}$$

The spectrum of the modal wind load $\boldsymbol{S}_{QQ}$ is obtained using the mode shapes $\boldsymbol{\Phi}$ of the bridge deck:

$$\boldsymbol{S}_{QQ}(f) = \int_0^L\int_0^L \boldsymbol{\Phi}(y_1)\boldsymbol{S}_{qq}(y_1, y_2, f)\boldsymbol{\Phi}(y_2)\mathrm{d}y_1\mathrm{d}y_2 \tag{11}$$

The power spectral density of the bridge response at abscissa y_r of the bridge is consequently:

$$\boldsymbol{S}_{y_r}(f) = [\boldsymbol{\Phi}(y_r)\cdot\boldsymbol{H}(f)]\cdot\boldsymbol{S}_{QQ}(f)\cdot[\boldsymbol{\Phi}(y_r)\cdot\boldsymbol{H}(f)]^{\mathrm{T}} \tag{12}$$

where $\boldsymbol{H}$ is the mechanical admittance of the system modified by the modal aerodynamic damping and stiffness. The standard deviation of the bridge displacement $\boldsymbol{\sigma}(y_r)$ at abscissa y_r is:

$$\boldsymbol{\sigma}(y_r) = \sqrt{\int_0^\infty \boldsymbol{S}_{y_r}(f)\mathrm{d}f} \tag{13}$$

where

$$\boldsymbol{\sigma}(y_r) = [\,\sigma_x(y_r)\quad\sigma_z(y_r)\quad\sigma_t(y_r)\,]^{\mathrm{T}} \tag{14}$$

In the present study, the cross-sectional aerodynamic admittance functions for the lift and drag forces, which are mainly concentrated at relatively long bridge eigen-periods, are taken equal to one for all frequencies. The cross-sectional aerodynamic admittances for the pitching moment, denoted $\chi_{\theta u}$ and $\chi_{\theta w}$, are traditionaly approximated using the Liepmann's approximation of the Sears' function

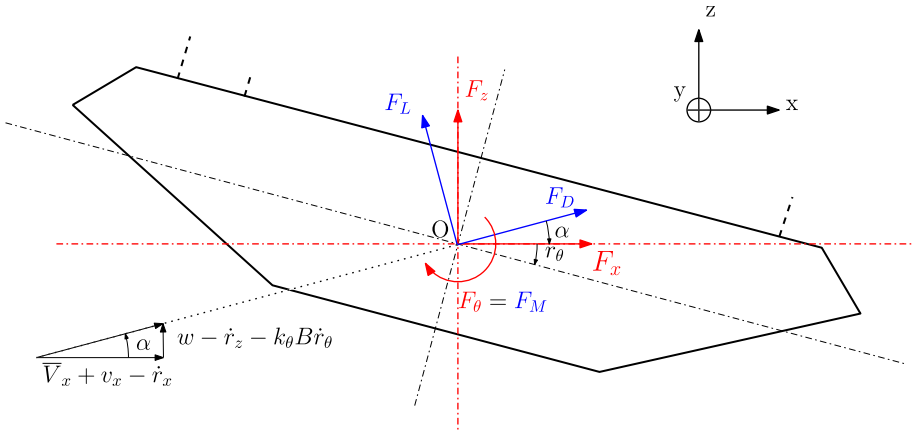

Fig. 3. Cross section of the bridge deck subjected to wind load.

[36], developed for a lift slope of 2π in a fully correlated sinusoidal gust (Eq. (15)). This cross-sectional admittance function was found to be better suited for the Lysefjord Bridge deck than the one introduced by Holmes [37] and used by e.g. by Matsuda et al. [38] for the pitching moment.

$$|\chi_{\theta u}(f)|^2 = |\chi_{\theta w}(f)|^2 = \frac{1}{1+\frac{2\pi f B}{\overline{V}_x}} \tag{15}$$

The verification of the buffeting theory is done by studying first the standard deviation of the bridge displacement response. More precisely, σ_x/I_u, σ_z/I_w, and σ_t/I_w are expressed as a function of the mean wind velocity component normal to the deck. The division by the turbulence intensity aims to reduce the dispersion of the data [16]. Then, the power spectral density (PSD) of the measured bridge response is compared to the one obtained by numerical simulation using a frequency domain approach. The PSD of the buffeting response is computed for the resonant part only, i.e. for frequencies above 0.08 Hz (lateral and vertical motions) and 0.24 Hz (torsional motion), since accelerometers generally provide less accurate data at lower frequencies [39]. In other words, the comparison between the measured and computed displacements concerns the resonant response only.

The modal parameters of the girder are summarized for the first 6 modes in each direction. The mode shapes are identified in the present study using the code XYZ, where X = {H, V, T} represents the lateral (H), vertical (V) or torsional (T) degree of freedom. Y = {S, A} is the symmetric (S) or asymmetric (A) feature of the mode shape, and Z is a digit representing the mode number. For example, HS1 refers to the first symmetric horizontal mode shape, and TA2 refers to the second asymmetric torsional mode shape. The deck dimensions, mechanical properties and its quasi steady aerodynamic coefficients are summarized in Table 3. The undamped mode shapes are computed in terms of Fourier series. For a more complete description of the bridge properties see e.g. [40].

6. Results and discussions

6.1. Modal analysis

The mode shapes and eigen-frequencies were computed by using every record of the bridge acceleration response on 07 and 26 October, corresponding to 287 samples of 10-min duration. The first symmetric and the first asymmetric mode shapes in each direction are compared to those provided by Alvsat. On Fig. 4, the four dots refer to the accelerometers located near H-09, H-18, H-24 and H-30, with the abscissa taken with reference to the North tower. The assumption of uncoupled mode shapes appears to be acceptable in view of the good agreement seen in Fig. 4. The measured eigen-frequencies also agree well with the computed ones (Table 4), where the largest error, of about 6%, is obtained for TS1. The higher modes HS2, HA2, VS2 and VA2 were clearly identified by the automated SSI-COV procedure, but are not included in this section for the sake of brevity. However, only the first two torsional modes TS1 and TA1 were identified.

Table 4
Comparison of the eigen-frequencies calculated using the SSI-COV method with the values provided by Alvsat software.

	SSI-COV (Hz)	Alvsat (Hz)	Difference (%)
HS1	0.133	0.130	−2.268
HA1	0.438	0.442	0.942
VA1	0.222	0.213	−3.948
VS1	0.293	0.286	−2.313
TS1	1.234	1.154	−6.421
TA1	2.180	2.125	−2.550

The measured modal damping ratios of the Lysefjord Bridge are studied statistically in the present study, because their values are affected by environmental conditions such as temperature variations, wind velocity fluctuations, or heavy traffic. Here, only the influence of the wind velocity is of interest, and the modal damping ratios were therefore bin-averaged as a function of the mean wind speed. Samples detected as non-stationary using the test from Bendat and Piersol [41] and samples characterized by a turbulence intensity larger than 30% were dismissed, as the estimation of the modal damping ratios requires the assumption of flow stationarity. The stationary test used, also referred to as the reverse arrangement test, was conducted by considering samples of 10 min and frequencies lower than 2 Hz. On 07/10/2014, ca. 56% of the samples were detected as non-stationary, whereas the ratio was only 7% on 26/10/2014. The high ratio of non-stationary records for the wind from N-NE is mainly related to the high turbulence intensity recorded induced by the complex topography on the East of the bridge. The mean value and standard deviation of the measured modal damping ratios are denoted $\overline{\zeta}$ and σ_ζ respectively, and are compared to theoretical values predicted by the quasi steady theory in Fig. 5.

Measured modal damping ratios larger than 5% or lower than 0.1% were dismissed for the sake of clarity. The first symmetric and asymmetric modes for the lateral, vertical and torsional bridge motion were selected for presentation. Larger values of σ_ζ are obtained for HS1, VA1 and VS1, which is explained by the relatively short duration of the acceleration records. A slightly non-linear evolution of the modal damping ratio for VA1 and VS1 is visible, likely reflecting the unsteady flow conditions, similarly to what was observed by Macdonald et al. [42] for a 948-m long cable stayed bridge. For TS1, HA1 and TA1, a remarkably low scatter of the modal damping ratios is obtained, and agrees well with the predicted values. Similar observations were done for the higher

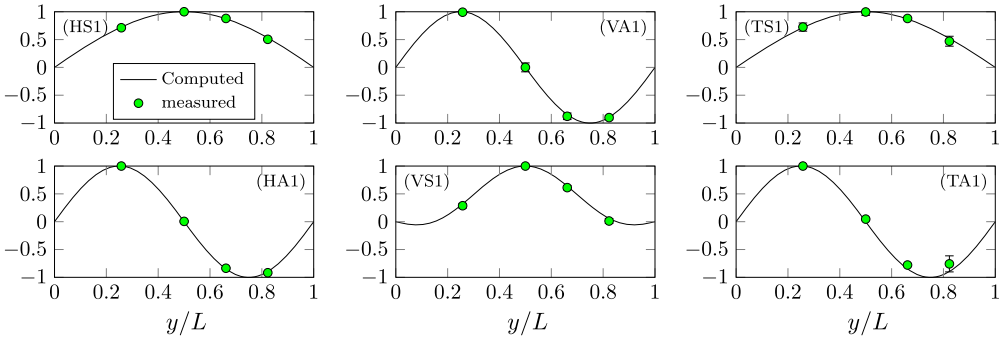

Fig. 4. Measured and computed mode shapes for the first two eigen-modes of Lysefjord Bridge based on acceleration records from 07/10/2014 and 26/10/2014. The small error bars show a low scatter of the identified mode shape.

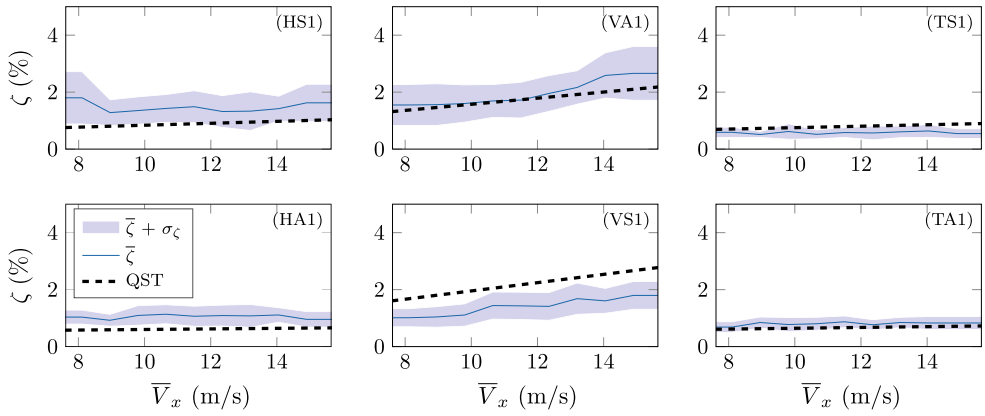

Fig. 5. Theoretical, measured and modal damping ratio from the Quasi-Steady Theory (QST) for the first two eigen-modes of Lysefjord Bridge based on acceleration records on 26/10/2014.

modes HS2, HA2, VS2 and VA2, with a modal damping ratio hardly increasing with the mean wind velocity. Fig. 5 shows in addition that the value $k_\theta = 0.25$ was a pertinent choice, given the good agreement between evolution of the predicted and measured total modal damping ratios for the torsional motion of the deck.

Previous analysis of the evolution of the modal damping ratios of suspensions bridges with wind velocity by e.g. Siringoringo et al. [43] have shown that the large scatter of the values observed for the low-frequency modes is to be expected. Longer samples may be used to reduce the dispersion of these modal damping ratios. However, the validity of the assumption of stationary wind fluctuations decreases for longer records [44]. For wind-sensitive structures, this assumption is fundamental to properly describe the evolution of the modal damping ratios with the mean wind velocity. For future ultra-long span suspension bridges, these contradictory requirements may challenge proper identification of the low-frequency modes.

6.2. Mean flow statistics

The wind field is studied in the "wind-based" coordinate system (u, v, w). Two dominant wind directions are observed, as summarized in Fig. 6 for two storms, i.e. on 26/10/2014 and 07/10/2014 respectively. The main wind direction on 07/10/2014 was N-NE with a mean value of 22° and a standard deviation of almost 9°. A high turbulence intensity was recorded that day, especially when the wind direction approached North. On 26/10/2014 the dominant wind direction was S-SW with a mean value of 211°, and a standard deviation of 6°. A much lower turbulence intensity was recorded, with no particular heterogeneity, opposite to what was observed in the N-NE wind situation case. The turbulence intensity for the N-NE wind is in average higher than those obtained by Hui et al. [8] for the open-land exposure, whereas for the S-SW wind, the turbulence intensity is closer to Hui's observations. The average ratio between I_w and I_u is equal to 0.41 and 0.57 for the N-NE and S-SW wind respectively, while a value of 0.55 is suggested by Holmes [45]. For the open-land exposure, Hui et al. [8] observed a value of 0.61, which once again is closer to what is recorded for the S-SW direction than for the N-NE direction. Turbulence intensity is particularly high for wind coming from North, which may be due to a possible partial flow descent from the mountains. Because these two wind conditions display different properties, the wind-induced response of the bridge has been studied using a case-by-case approach, i.e. by separating the flow from S-SW and the one from N-NE.

For the N-NE wind, 90% of the wind records displayed a negative incidence angle below 1.7° suggesting a negligible influence of the wind incidence angle on the bridge response. For the wind

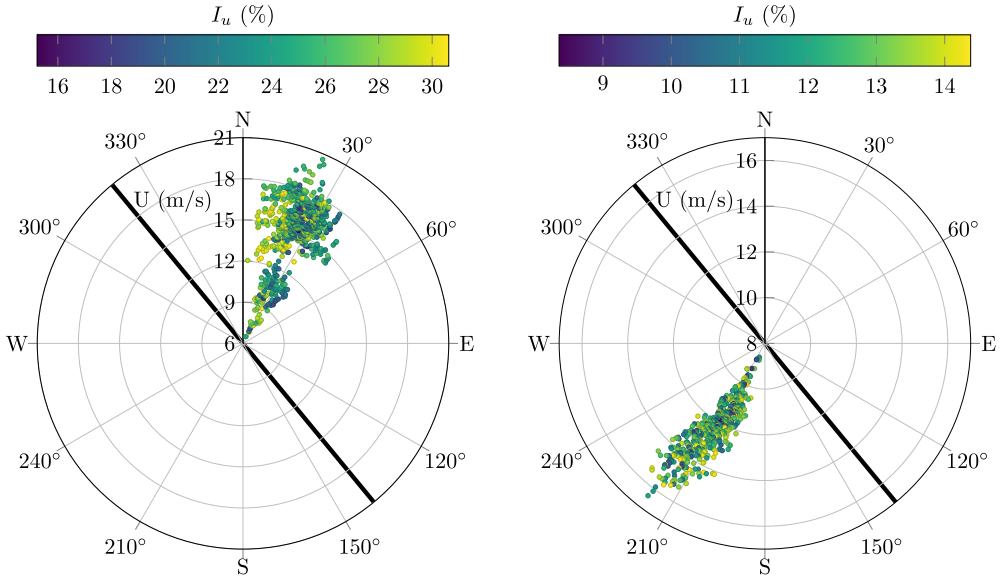

Fig. 6. Two dominating wind conditions usually observed at Lysefjord Bridge: 07/10/2014 to the left and 26/10/2014 to the right. The thick black line indicates the bridge orientation. Each dot represents 10 min of averaged wind data.

from S-SW, larger positive wind incidence angle were detected up to 7°. No clear relationship between the incidence angles and the observed responses was identified. Possible origins of the high values of the incidence angles are discussed in Section 7.

6.3. Single point statistics

The single-point statistics of wind turbulence is studied in the wind-based coordinate system to compare the recorded data with the semi-empirical counterpart. On Figs. 7 and 8, the von Kármán spectrum [27] agrees well with the measured spectra for the along and across-wind components, both for a wind from N-NE and S-SW, for the wavenumber range of interest, i.e. higher than 0.08 m^{-1}. The measured vertical spectra is however larger than the computed one for wavenumbers larger than 0.02 m^{-1}. The Kolmogorov hypothesis for the inertial subrange predicts a value of 4/3 for the ratios S_w/S_u and S_v/S_u. This was observed by Kaimal et al. [46] for flat and homogeneous terrains, although the dependency on the atmospheric stability was strong. In the present case, these relations are not verified when the data from the anemometer located 6 m above the deck (H-08b) is used. For the wind from S-SW, S_v/S_u is almost equal to 1 in the inertial subrange whereas S_w/S_u shows a sudden increase from 1.4 to 2.2 between $k = 0.05\ m^{-1}$ and $k = 5\ m^{-1}$. For the N-NE exposure, S_v/S_u is around 1.5 in the inertial subrange but S_w/S_u is much larger.

The anemometers are all installed on the West side of the bridge deck, which may particularly disturb the recorded flow in the N-NE wind situation. The ratio between the wind spectra recorded on H-08b (6 m above the deck) over H-08t (10 m above the deck) is therefore calculated for both exposure, and directly compared (Figs. 9 and 10). Whatever the wind exposure, the records of the along-wind component seem to be relatively little affected by the deck. For the vertical wind component and for the N-NE wind case situation, this ratio increases up to 1.3 for $k = 1\ m^{-1}$. For $\overline{U} = 14.8$ m/s, $k = 0.1\ m^{-1}$ corresponds to $f = 0.24$ Hz. The amplified spectral content in the higher frequency range for the N-NE direction is likely due to the bridge signature turbulence linked to the location of the anemometers. The island of Bergsholmen, located 1 km on the East of the bridge reaches

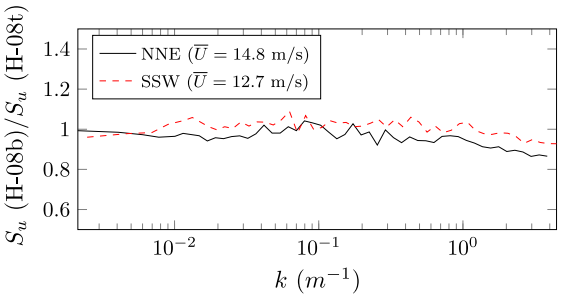

Fig. 9. Influence of the bridge deck on the along-wind component *u*.

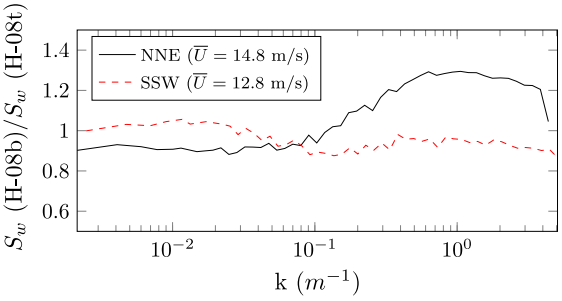

Fig. 10. Influence of the bridge deck on the vertical wind component *w*.

an altitude of 54 m. When the wind direction reaches ca. 25°, the flow recorded by the anemometers has crossed the island prior to "hitting" the bridge. When the wind direction fluctuates between 5° and 25°, the wind flows between the cliff of the fjord and Bergsholmen, and may be accelerated by the sudden narrowing of the fjord 1 km upstream of the bridge. Abrupt topographical changes may consequently modify both the wind profile and the ratio S_w/S_u.

6.4. Two point statistics

The co-coherence has been calculated in the bridge-based coordinate system, using the Welch's spectral estimation [47], based on

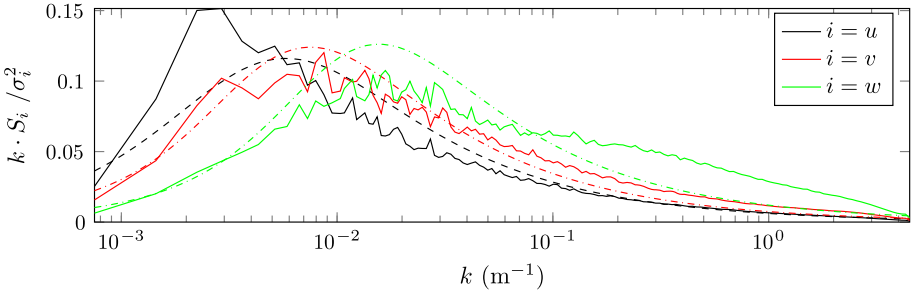

Fig. 7. Averaged wind spectra recorded on 07/10/2014 for a N-NE wind (solid lines) and corresponding von Kármán spectra (dashed lines).

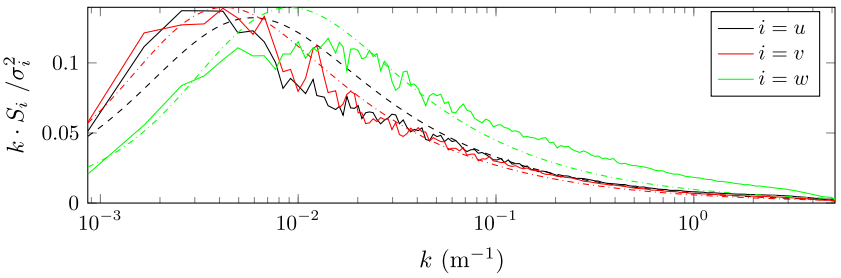

Fig. 8. Averaged wind spectra recorded on 26/10/2014 for a S-SW wind (solid lines) and corresponding von Kármán spectra (dashed lines).

data of 10 min that are divided into two blocks of 5 min each, a Hamming Window and 50% overlapping, as suggested by [48,49]. For a given frequency and a given spatial separation, the co-coherence is averaged for every sample recorded during one day, i.e. 144 samples. The coefficients for the co-coherence function represented by Eq. (4) are calculated using curve fitting techniques for distances ranging from 24 m to 168 m. The coefficients evaluated during the curve fitting, by using the bridge-based coordinate system, are presented in Table 5. The measured and fitted co-coherence are expressed as a function of the wavenumber k which is expressed as a function of $\overline{V}_x$ instead of $\overline{U}$. The co-coherence is displayed for three different lateral separations on Figs. 11 and 12.

Table 5
Decay coefficients measured on 26/10/2014 and 07/10/2014 for lateral separation along the span.

Exposure	Component	Decay coefficients			
N-NE	v_x	$c_1 = 5.0$	$c_2 = 0.07$	$c_3 = 1.1$	$c_4 = 3.3$
	w	$c_1 = 4.7$	$c_2 = 0.08$	$c_3 = 1.2$	$c_4 = 2.0$
S-SW	v_x	$c_1 = 6.5$	$c_2 = 0.02$	$c_3 = 0.9$	$c_4 = 6.7$
	w	$c_1 = 7.9$	$c_2 = 0.1$	$c_3 = 1.1$	$c_4 = 5.4$

The overall surface-fitting process shows satisfying results, although some non-negligible differences between a N-NE wind and a S-SW wind can be observed. The co-coherence for a wind from N-NE is larger than for a wind from S-SW, as highlighted by the coefficient c_1. For small distances and wavenumbers above 0.02 m^{-1}, the fitted co-coherence for the v_x-component of N-NE wind, did not compare well with the measured co-coherence. The negative part of the co-coherence is taken into account but has little consequence on the overall shape of the fitted function. The values of the coefficients in Table 5 are used in Section 6.5 and 6.6 for the computation of the buffeting response of the Lysefjord Bridge.

6.5. Buffeting response at mid-span

The buffeting response is evaluated based on 144 samples of 10-min wind data and displacement response recorded on 26/10/2014 and on 07/10/2014. The wind field is assumed homogeneous along the span, and therefore, the mean wind speed and wind spectra measured near the bridge center on H-18 and H-20 are averaged. The standard deviation of the measured and com-

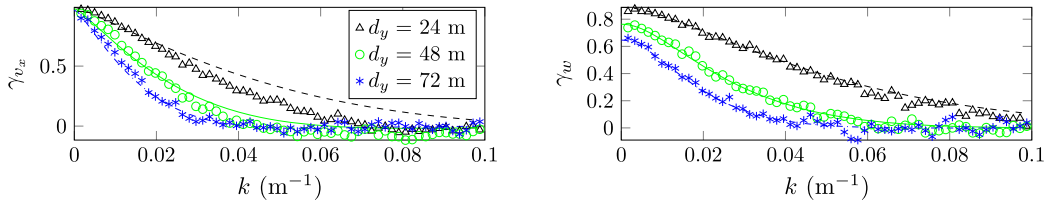

Fig. 11. Measured (scatter plot) and fitted co-coherence (solid and dashed lines) for the v_x- and w-components. An averaged coherence is calculated, based on every wind data recorded on 07/10/2014 (N-NE exposure), with $\overline{V}_x = 12.6$ m/s.

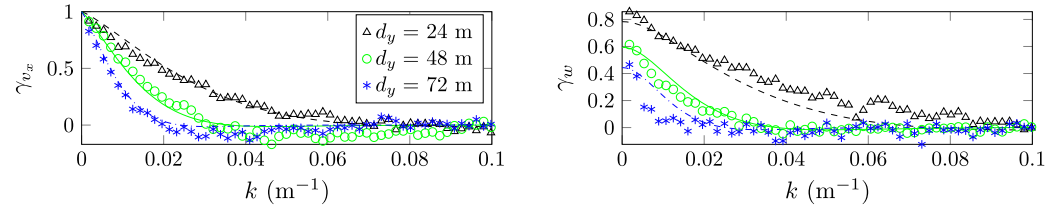

Fig. 12. Measured (scatter plot) and fitted co-coherence (solid and dashed lines) for the v_x- and w-components. An averaged coherence is calculated, based on every wind data recorded on 26/10/2014 (S-SW exposure), with $\overline{V}_x = 11.8$ m/s.

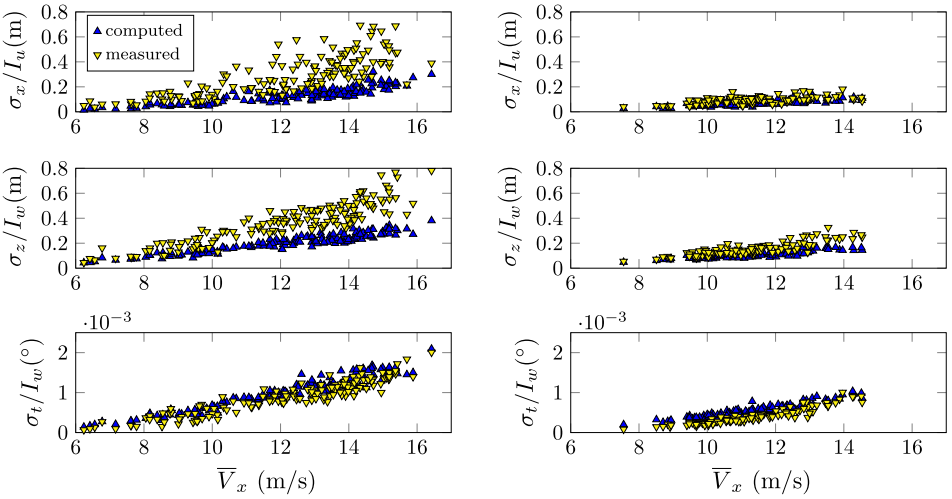

Fig. 13. RMS of the bridge deck response at mid-span for a N-NE wind (left panels) and a S-SW-wind (right panels).

puted bridge displacement are expressed as a function of the mean wind speed normal to the bridge deck (Fig. 13). The RMS of the displacement has been normalized by the corresponding turbulence intensity to reduce the spreading of the data. A good overall agreement is found between the measured and computed RMS values, especially for S-SW wind. The simulated RMS values underestimate the normalized RMS response for N-NE wind for the lateral and vertical motions. For a given wind velocity, the RMS of the bridge displacement is generally higher for a N-NE wind than for a S-SW wind, which is characterized by a lower turbulence intensity and a lower co-coherence.

6.6. Buffeting response along the span

Among all the wind records, one single sample is selected. Its stationarity is assessed by using the test from Bendat and Piersol [41], and its mean wind velocity is taken as large as possible, so that the bridge response is mainly due to wind turbulence rather than by traffic induced vibrations [50]. For the sake of simplicity, the co-coherence coefficients and cross-sectional aerodynamic admittance functions are the same as in subSection 6.5. The measured wind spectra are directly used as inputs to compute the buffeting response of the bridge. Under the wind conditions considered, mode coupling induced by the wind load is found to be insignificant for the structure, which is consistent with [51,52], and is therefore neglected. The shear center of the bridge cross-section is located 0.4 m below the neutral axis [53], which induces an additional structural coupling between the lateral and torsional motions of the bridge deck. However, it has small effects on the overall response and was therefore neglected. The properties of the wind sample selected for each wind exposure are displayed in Table 6. The RMS of the computed bridge response on H-09, H-18, H-24 and H-30 is compared to the measured one on Fig. 14. The computed RMS of the bridge response agrees well for the S-SW wind exposure, but underestimates the bridge response in the N-NE wind case situation. The simulated response displays a symmetry with respect to the mid-span, which is not the case for the measured response. The bridge deck is indeed not symmetric: the Northern end and the middle part of the span are respectively 8 and 13 m higher than the Southern end. In addition, the wind field is assumed homogeneous along the deck, whereas the wind spectra may display non-negligible variations along the span. The approach based on using averaged spectra to compute the wind load may therefore not be satisfactory. The assumption of homogeneity may be acceptable for a S-SW wind, but not for the N-NE wind situation case, where a higher mean wind speed is often observed towards the North tower.

A more detailed description of the bridge response near H-24 is shown in Fig. 15. The main sources of discrepancy are the computed resonant peaks that sometimes disagree with the measured ones in terms of broadness and/or amplitude. Different possibilities for these discrepancies are investigated in details in Section 7. Beyond the third or fourth mode for each direction, these discrepancies have a negligible influence on the overall response of the bridge. For the torsional motion, the mode TS1 is dominant, such as the overestimation of the modal response for TA1 has little consequences on the computed torsional displacement. The overestimation of the computed modal response for TA1 is likely due to the choice of the cross-sectional aerodynamic admittance function that did not fit well with the one obtained from the recorded data at frequencies larger than 1.8 Hz.

Table 6
Properties of the selected wind sample for the computation of the buffeting response on Fig. 14.

Exposure	NNE	SSW
$\overline{U}$ (m/s)	17.7	13.9
$\overline{V}_x$ (m/s)	14.7	12.9
I_u	0.26	0.15
I_v	0.21	0.15
I_w	0.11	0.08
L_u (m)	220	202
L_v (m)	83	120
L_w (m)	41	73

7. Challenges and prospects

The measured bridge response due to the flow from N-NE is systematically larger than for the S-SW wind case situation. The increase of the measured wind coherence and turbulence intensity leads to a larger computed buffeting response, which yet remains lower than the measured one. In the following discussion several

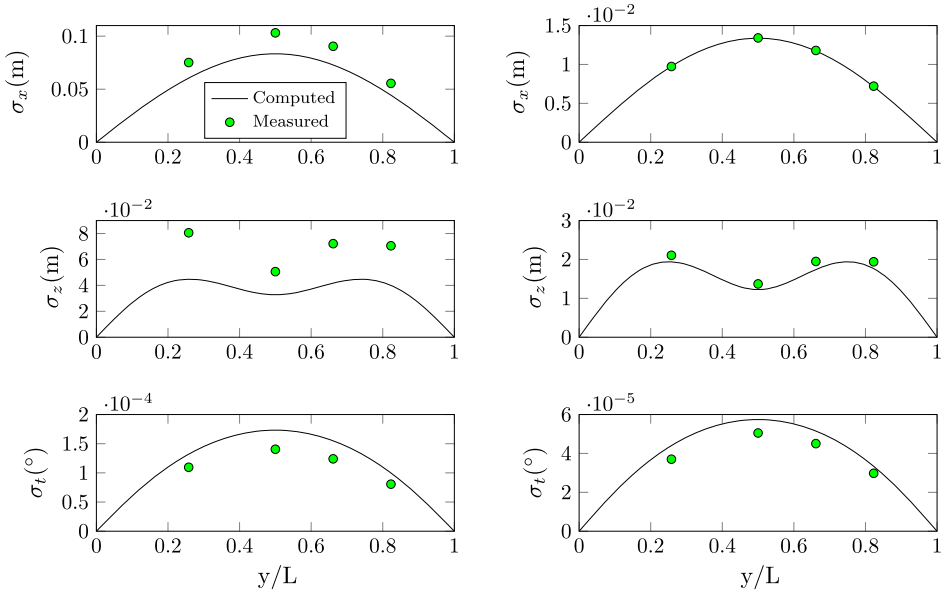

Fig. 14. RMS of the deck response for a N-NE wind (left panels, on 07/10/2014 at 09:20) and a S-SW-wind (right panels, on 26/10/2014 at 08:50), see Table 6.

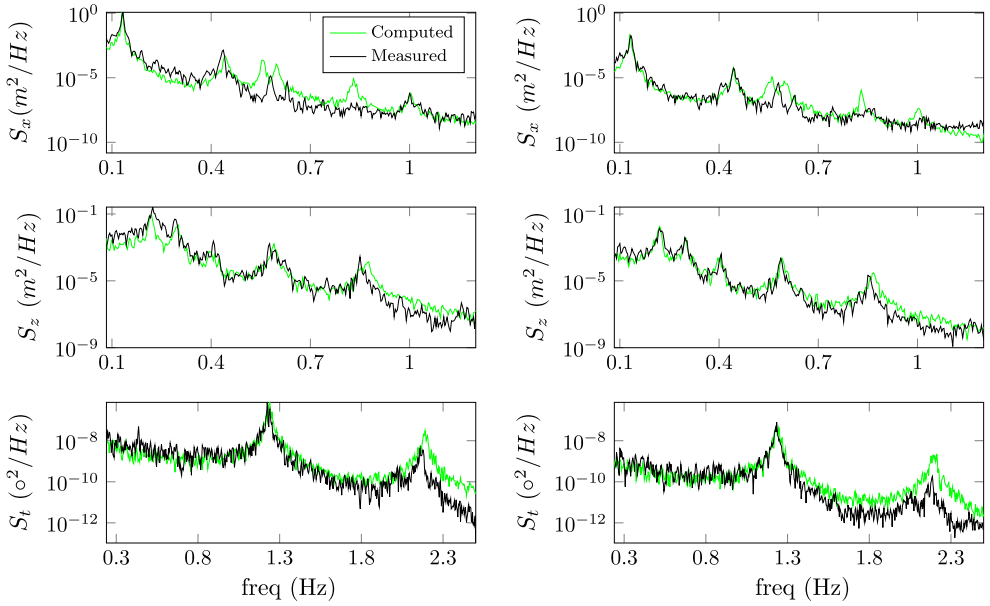

Fig. 15. PSD the deck displacement response near H-24, for the N-NE wind case (left panels, on 07/10/2014 at 09:20) and a S-SW-wind case (right panels, on 26/10/2014 at 08:50) described in subSection 6.6.

issues are explored that may influence or explain the differences observed in the response for the two dominating wind directions, as well as the discrepancies between the computed and measured response.

7.1. Influence of the yaw angle

The influence of the yaw angle on the bridge response was considered by directly using the measured wind component normal to the bridge deck V_x instead of the along-wind component U. This method, referred to as the "cosine rule", was applied by e.g. Tanaka and Davenport [54], but for relatively small turbulence intensities only. Although this method is simple, it does not consider the variation of the aerodynamic coefficients with the yaw angle [55], which may lead to an inaccurate estimation of the buffeting response. More generally, deviations from the cosine rule have been previously observed in wind tunnel, in particular at large yaw angles [56,57]. The measured displacement data for the lateral displacements in N-NE winds shows greater variability than seen for the other response components. Zhu et al. [57] have shown that the RMS of the lateral bridge response is likely to be more influenced by the yaw angle than the torsional and vertical response.

Figs. 16 and 17 show that the "cosine rule" does not apply systematically in the case of the Lysefjord bridge. The influence of the topography on the flow actually plays a predominant role. For the S-SW exposure, larger yaw angles are associated with lower wind

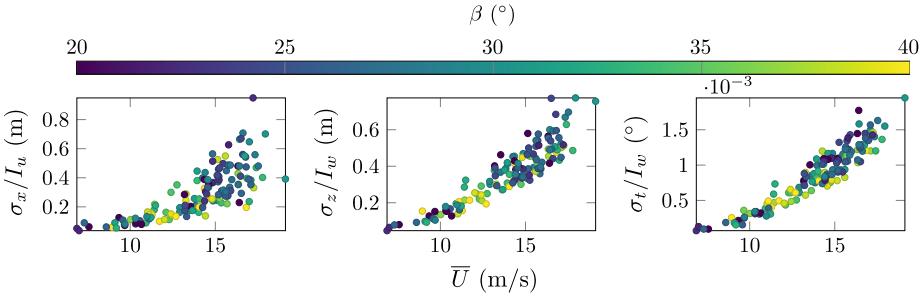

Fig. 16. Influence of the yaw angle on the measured buffeting response of the Lysefjord Bridge (N-NE exposure and wind data from H-18).

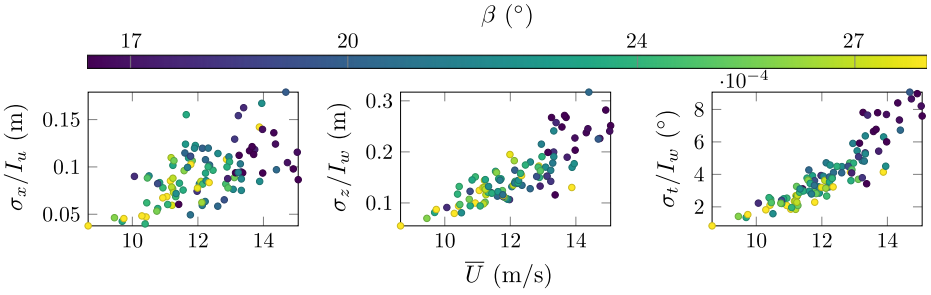

Fig. 17. Influence of the yaw angle on the measured buffeting response of the Lysefjord Bridge (S-SW exposure and wind data from H-18).

velocities, corresponding to a wind from South flowing along the mountains surrounding the fjord. For the wind from N-NE, there is no clear relation between the yaw angle, the along-wind mean wind velocity, and the bridge response. Particularly large yaw angles recorded for the wind from N-NE may lead to a measured displacement much larger than expected. However, the discrepancies between the measured response for the two exposure studied can not be explained by the influence of the yaw angle on the bridge response only. A more rigorous analysis of the buffeting response of the Lysefjord Bridge for the N-NE wind should therefore include the study of the evolution of the aerodynamic coefficients with the yaw angle, in a similar fashion as in [55].

7.2. Contribution of the bridge towers and main cables to aerodynamic loading

The computation of the bridge response has been done by considering the wind load on the bridge deck only. For the Tsing Ma Bridge, Xu et al. [58] have observed an increase up to 15% of the computed buffeting lateral response at mid span when the buffeting load was applied to the whole structure (deck, tower and main cables). For the Lysefjord Bridge, the main cables consist of 6 individual cables installed next to each other, each with the 0.1 m diameter. With the drag coefficient of 2 applied to the whole cable group, the mean drag load on the main cable accounts for 7% of the total one on the bridge. Large discrepancies between the computed and measured lateral displacement response are therefore unlikely to be due to the influence of the bridge towers and main cables on the deck lateral motion.

7.3. Influence of the bridge deck on the measured wind data

For the anemometers located at $z = 6$ m and $z = 10$ m above the deck, the ratio z/H is equal to 2.2 and 3.6 respectively. For the N-NE exposure the recorded wind velocities may be affected by the girder, leading to a inaccurate estimation of the bridge response. The possible influence of a bridge deck on the mean flow recorded by anemometers has been investigated by [59,60]. Kristensen et al. [59] used sonic anemometers mounted 3 m above the deck of the Sotra Bridge (truss-type girder), whereas Frandsen [60] used cup anemometer installed 2 m above the deck of the Great Belt Bridge (closed-box girder). None of them found that the mean wind velocity was significantly affected by the deck, and they assumed that the measured flow was representative of the upstream one. Their investigations may have been incomplete regarding this issue. In the present case, the sonic on H-08t measures a mean wind velocity in average 2.3% lower than at H-08b for the N-NE exposure, whereas the difference is less than 1% when the wind comes from S-SW. This indicates that the mean flow may be affected to a non-negligible extent by the deck. Similarly, a somewhat larger coherence for the N-NE may reflect an influence of the bridge deck on the recorded velocity data. Such details will be scrutinized in a future study, by introducing additional sonic anemometers on the East side of the bridge. Nonetheless, the results extracted from the data at hand provide the insightful and systematic relationship between the Wind conditions and the bridge deck vibrations.

No particular relation was observed between the incidence angle and the bridge response. The large incidence angles observed for the wind from S-SW may also be due to the influence of the deck on the measured vertical flow. This may also explain the somewhat untraditional values measured for the ratio S_w/S_u and S_v/S_u in the inertial subrange (subSection 6.3).

7.4. Validity of the assumption of homogeneous flow

The assumption of non-homogeneity of the flow can be introduced in the present numerical model by defining at each "node" of the discrete bridge deck model a different power spectral density obtained by linear interpolation and extrapolation of the measured spectra. If the non-uniformity of the mean wind velocity is not too large, the coherence model can remain unchanged. Fig. 18 shows the computed standard deviation of the bridge displacement where the wind spectra used as input is based on one single anemometer, located either on H-08b, H-08t or H-18. The discrepancy of the computed response due to the choice of the reference sensor is expected, as seen in subsection 7.3. The wind records on H-08b and H-18 are different enough to be responsible for a non-negligible difference between the computed responses, which suggests that the assumption of homogeneous flow is not necessary verified for the N-NE wind case situation. Further analysis should re-assess the validity of the assumption of flow uniformity on a more systematically way. For ultra-long span suspension bridges in mountainous environments, the lack of flow uniformity along the span may call for a modified design approach.

7.5. Non-stationarity of the flow

The stationarity test of Bendat and Piersol [41] has been previously applied by Chen et al. [61] to assess the non-stationarity of wind velocity data. In the present study, a non-negligible amount of samples did not pass this test. Other indicators of the non-stationary flow may be unrealistic large turbulence length scales, high turbulence intensities, and large variations of the wind direction. New approaches to characterize wind turbulence for non-stationary flow may be required. Hu et al. [62] have for example used time-varying single-point statistics to estimate the buffeting response of a long-span suspension bridge, and observed that non-stationary buffeting response could be larger than predicted by the stationary model. In the present study, we observed that non-stationary wind fluctuations were often associated with a larger scatter of the buffeting response, in particular in the case of the lateral bridge motion. We observed in addition that the computation of the lateral bridge displacement by using directly the PSD

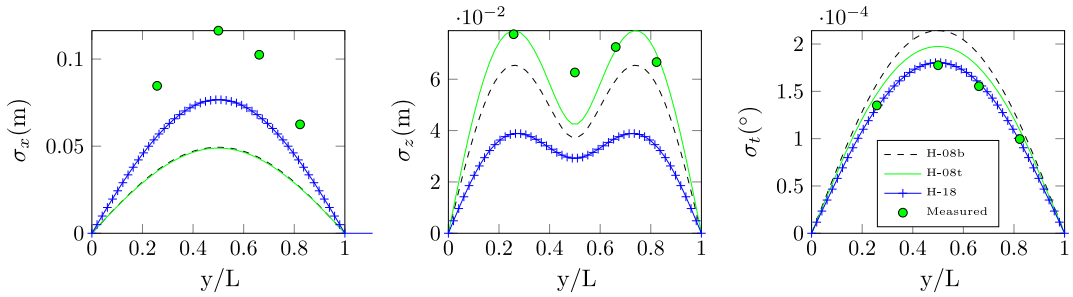

Fig. 18. Influence of the choice of the reference anemometer on the computed bridge response for the N-NE wind case situation (on 07/10/2014 at 03:50:00).

of the non-stationary wind fluctuations tends to underestimate the real displacement. A similar issue was observed for stationary wind data by Chen et al. [63] when they compared the frequency and time domain approach to compute the lateral buffeting response of a numerical bridge model. In full scale, this numerical issue may be overcome by using an empirical model for the PSD that is fitted to the measured one, as done by Xu et al. [5].

7.6. Influence of traffic induced vibrations

The influence of traffic-induced vibrations can generally be neglected for wind speeds higher than 12 m/s [50]. For lower wind velocities, unexpected large amplitude of vibrations are often due to heavy traffic, leading to a measured response larger than predicted by the buffeting theory. For the data studied, the variance of the measured bridge displacement did not display any sudden variations at lower wind velocities. This indicates that the large displacements measured for the flow from N-NE are unlikely to be due to heavy traffic.

7.7. Influence of the u–w cross-spectral densities

We did not include the in-phase co-spectrum Co_{uw} of wind fluctuations into the matrix of wind load in the present study, since its contribution on the bridge response was lower than 0.3% in average. This is in agreement with Øiseth et al. [64] who observed that the contribution of the co-spectrum to the dynamic response of a suspension bridge was likely to be low compared to the uncertainties related to the modeling of the bridge and wind turbulence properties.

7.8. Non-linear effects of the wind load

By assuming uncoupled motions of the Lysefjord Bridge, the variance of the error due to the linearization of the wind load for the vertical motion is:

$$\eta^2 = 1 + \frac{\sigma_{\mathrm{nL}}^2}{\sigma_{\mathrm{L}}^2} \tag{16}$$

where σ_{L}^2 and σ_{nL}^2 are the variance of the vertical wind load without and with introduction of the quadratic terms respectively. Applying the Taylor series expansion up to order 2 of the derivatives of the force coefficients with respect to the angle of attack, we can rewrite Eq. (16) as:

$$\eta^2 = \frac{1}{2}\left[1 \quad \frac{C_L + C_L'' + 2D/B \cdot C_D'}{C_L' + D/B \cdot C_D}\right] \cdot \begin{bmatrix} 2I_u^2 \\ 2I_w^2 \end{bmatrix} \tag{17}$$

where C_L'' is the second derivative of the the lift coefficient with respect to the incidence angle. For the Lysefjord bridge, $C_D' = 0$. Assuming that the vertical turbulence intensity I_w is proportional to the along-wind one I_u with a proportionality constant $\delta < 1$, and by assuming that $C_L'' \simeq 0$, Eq. (17) becomes:

$$\eta^2 = 1 + \frac{I_u^2}{2}\left\{1 + \left[\delta \cdot C_L \Big/ \left(C_L' + \frac{D}{B} C_D\right)\right]^2\right\} \tag{18}$$

$$\simeq 1 + \frac{I_u^2}{2} \tag{19}$$

The standard deviation for the error is therefore:

$$\eta \simeq 1 + \frac{I_u^2}{4} \tag{20}$$

A similar result is found by Denoël [65, p. 136]. For a turbulent intensity of 0.3, the standard deviation of the error on the vertical load, introduced by neglecting the quadratic terms of the wind fluctuations remains consequently below 3% in the present case. For the measured vertical bridge displacement response, the large difference between the S-SW and the N-NE wind case situation cannot be explained by the non-linearity of the wind load only.

8. Conclusions

The present study compared the theoretically estimated buffeting response and the measured response of a long span bridge in a complex terrain. Two unique sets of 24-h of continuous data were used for this purpose. The first data set was made of wind records from a stable direction from S-SW, with wind velocities ranging from 8 m/s to almost 17 m/s. The second data set corresponded to flow from N-NE with velocities data ranging from 6 to 21 m/s. The analysis has been carried out in three steps to provide an analysis as complete as possible in full-scale:

1. A modal identification analysis was first applied as a verification procedure by using an automated SSI-COV procedure. We observed a good agreement between the computed and measured mode shapes and eigen-frequencies. The estimation of the total modal damping ratio was done in a statistical manner, and despite a scatter of the data for HS1, VA1 and VS1, a general consistency with the quasi-steady theory was observed.
2. The analysis of the wind conditions at Lysefjord has been undertaken, and two main directions were observed. A large turbulence intensity for the N-NE wind is detected, which suggests a non-negligible influence of the topography on the flow. A four-parameter co-coherence function has been defined to properly capture the correlation of the wind load along the bridge. We concluded that the two main wind directions show different turbulence properties, which justifies a case-by-case approach. More generally, a case-by-case approach may be necessary for wind and structural health monitoring of long-span suspension bridges in complex terrains.
3. The buffeting response of the bridge deck has been studied first at the middle of the span for multiple wind records from two different storms, and then along the whole span for two particular wind records. To improve the response estimated based on the quasi-steady theory, the use of a cross-sectional aerodynamic admittance function for the torsional motion was found necessary. We observed that the Liepmann's approximation of the Sears' function is an applicable choice. The measured buffeting response of the bridge for a N-NE wind is considerably larger than the one for the S-SW exposure. The computed buffeting response agrees well with the S-SW wind case situation, but underestimates the lateral and vertical bridge displacement for the flow from N-NE. The main reasons of such discrepancies may be due to the influence of the topography on the flow, non-stationary wind fluctuations, and possible distortion of the observed flow by the bridge deck.

Acknowledgements

The support of the Norwegian Public Roads Administration is gratefully acknowledged, as well as their assistance during the installation and maintenance of the monitoring system.

References

[1] Davenport AG. The application of statistical concepts to the wind loading of structures. ICE proceedings, vol. 19. p. 449–72.
[2] Scanlan R. The action of flexible bridges under wind, II: Buffeting theory. J Sound Vib 1975;60(2):201–11. http://dx.doi.org/10.1016/S0022-460X(78)80029-7.

[3] Xu Y-L. Wind effects on cable–supported bridges. John Wiley & Sons Singapore Pte. Ltd.; 2013. p. 345–84. http://dx.doi.org/10.1002/9781118188293.ch9 [chapter 9].

[4] Bietry J, Delaunay D, Conti E. Comparison of full-scale measurement and computation of wind effects on a cable-stayed bridge. J Wind Eng Indust Aerodynam 1995;57(2):225–35. http://dx.doi.org/10.1016/0167-6105(94)00110-Y.

[5] Xu Y, Zhu L. Buffeting response of long-span cable-supported bridges under skew winds. Part 2: Case study. J Sound Vib 2005;281(35):675–97. http://dx.doi.org/10.1016/j.jsv.2004.01.025.

[6] Macdonald JH. Evaluation of buffeting predictions of a cable-stayed bridge from full-scale measurements. J Wind Eng Indust Aerodynam 2003;91(1215):1465–83. http://dx.doi.org/10.1016/j.jweia.2003.09.009.

[7] Hui M, Larsen A, Xiang H. Wind turbulence characteristics study at the Stonecutters Bridge site: Part II: Wind power spectra, integral length scales and coherences. J Wind Eng Indust Aerodynam 2009;97(1):48–59. http://dx.doi.org/10.1016/j.jweia.2008.11.003.

[8] Hui M, Larsen A, Xiang H. Wind turbulence characteristics study at the Stonecutters Bridge site: Part I: Mean wind and turbulence intensities. J Wind Eng Indust Aerodynam 2009;97(1):22–36. http://dx.doi.org/10.1016/j.jweia.2008.11.002.

[9] Wang H, Li A, Hu R. Comparison of ambient vibration response of the runyang suspension bridge under skew winds with time-domain numerical predictions. J Bridge Eng 2011;16(4):513–26. http://dx.doi.org/10.1061/(ASCE)BE.1943-5592.0000168.

[10] Toriumi R, Katsuchi H, Furuya N. A study on spatial correlation of natural wind. J Wind Eng Indust Aerodynam 2000;87(2):203–16. http://dx.doi.org/10.1016/S0167-6105(00)00037-4.

[11] Miyata T, Yamada H, Katsuchi H, Kitagawa M. Full-scale measurement of akashi–kaikyo bridge during typhoon. J Wind Eng Indust Aerodynam 2002;90(12):1517–27. http://dx.doi.org/10.1016/S0167-6105(02)00267-2.

[12] Wang H, Li A, Niu J, Zong Z, Li J. Long-term monitoring of wind characteristics at sutong bridge site. J Wind Eng Indust Aerodynam 2013;115:39–47. http://dx.doi.org/10.1016/j.jweia.2013.01.006.

[13] Nakamura S. Gps measurement of wind-induced suspension bridge girder displacements. J Struct Eng 2000;126(12):1413–9. http://dx.doi.org/10.1061/(ASCE)0733-9445(2000)126:12(1413).

[14] Brownjohn J, Bocciolone M, Curami A, Falco M, Zasso A. Humber bridge full-scale measurement campaigns 1990–1991. J Wind Eng Indust Aerodynam 1994;52:185–218. http://dx.doi.org/10.1016/0167-6105(94)90047-7.

[15] Nagayama T, Abe M, Fujino Y, Ikeda K. Structural identification of a nonproportionally damped system and its application to a full-scale suspension bridge. J Struct Eng 2005;131(10):1536–45. http://dx.doi.org/10.1061/(ASCE)0733-9445(2005)131:10(1536).

[16] Hay J. Analyses of wind and response data from the Wye and Erskine bridges and comparison with theory. J Wind Eng Indust Aerodynam 1984;17(1):31–49.

[17] Frank H. A simple spectral model for the modification of turbulence in flow over gentle hills. Bound-Layer Meteorol 1996;79(4):345–73. http://dx.doi.org/10.1007/BF00119404.

[18] Mann J. The spectral velocity tensor in moderately complex terrain. J Wind Eng Indust Aerodynam 2000;88(23):153–69. http://dx.doi.org/10.1016/S0167-6105(00)00046-5. International conference on wind engineering.

[19] Xie J, Tanaka H, Wardlaw R, Savage M. Buffeting analysis of long span bridges to turbulent wind with yaw angle. J Wind Eng Indust Aerodyn 1991;37(1):65–77. http://dx.doi.org/10.1016/0167-6105(91)90005-H.

[20] Kimura K, Tanaka H. Bridge buffeting due to wind with yaw angles. J Wind Eng Indust Aerodynam 1992;42(1):1309–20. http://dx.doi.org/10.1016/0167-6105(92)90139-2.

[21] Scanlan RH. Bridge buffeting by skew winds in erection stages. J Eng Mech 1993;119(2):251–69. http://dx.doi.org/10.1061/(ASCE)0733-9399(1993)119:2(251).

[22] Magalhães F, Cunha A, Caetano E. Online automatic identification of the modal parameters of a long span arch bridge. Mech Syst Signal Process 2009;23(2):316–29. http://dx.doi.org/10.1016/j.ymssp.2008.05.003.

[23] Magalhães F, Cunha A. Explaining operational modal analysis with data from an arch bridge. Mech Syst Signal Process 2011;25(5):1431–50. http://dx.doi.org/10.1016/j.ymssp.2010.08.001.

[24] Brownjohn J, Magalhaes F, Caetano E, Cunha A. Ambient vibration re-testing and operational modal analysis of the humber bridge. Eng Struct 2010;32(8):2003–18. http://dx.doi.org/10.1016/j.engstruct.2010.02.034.

[25] James III O, Came T, Lauffer J. The natural excitation technique (next) for modal parameter extraction from operating structures. Int J Anal Exp Modal Anal 1995;10(4):260–77.

[26] Peeters B, Van der Auweraer H, Guillaume P, Leuridan J. The polymax frequency-domain method: a new standard for modal parameter estimation? Shock Vib 2004;11(3–4):395–409. http://dx.doi.org/10.1155/2004/523692.

[27] Morfiadakis E, Glinou G, Koulouvari M. The suitability of the von Karman spectrum for the structure of turbulence in a complex terrain wind farm. J Wind Eng Indust Aerodynam 1996;62(2):237–57. http://dx.doi.org/10.1016/S0167-6105(96)00059-1.

[28] Panofsky HA, Brier GW, Best WH. Some application of statistics to meteorology. Earth and mineral sciences continuing education, College of Earth and Mineral Sciences, Pennsylvania State University; 1958.

[29] Davenport AG. The spectrum of horizontal gustiness near the ground in high winds. Quart J Roy Meteorol Soc 1961;87(372):194–211. http://dx.doi.org/10.1002/qj.49708737208.

[30] Vickery BJ. On the reliability of gust loading factors. Proc., technical meeting concerning wind loads on buildings and structures, building science series, vol. 30. p. 296–312.

[31] Jakobsen JB. Span-wise structure of lift and overturning moment on a motionless bridge girder. J Wind Eng Indust Aerodynam 1997;69:795–805. http://dx.doi.org/10.1016/S0167-6105(97)00206-7.

[32] Hjorth-Hansen E, Jakobsen A, Strømmen E. Wind buffeting of a rectangular box girder bridge. J Wind Eng Indust Aerodynam 42. doi:http://dx.doi.org/10.1016/0167-6105(92)90128-w.

[33] Krenk S. Wind field coherence and dynamic wind forces. In: IUTAM symposium on advances in nonlinear stochastic mechanics. Springer; 1996. p. 269–78. http://dx.doi.org/10.1007/978-94-009-0321-0_25.

[34] Von Kármán T. Progress in the statistical theory of turbulence. Proc Natl Acad Sci USA 1948;34(11):530.

[35] Irwin H, Wardlaw R. Wind tunnel and analytical investigations of the response of Lions' Gate Bridge to turbulent wind. national research council of canada. Tech. rep., NAE LTR-LA-210; 1976.

[36] Liepmann H. On the application of statistical concepts to the buffeting problem. J Aeronaut Sci 1952;19(2):793–800. http://dx.doi.org/10.2514/8.2491.

[37] Holmes J. Prediction of the response of a cable-stayed bridge to turbulence. In: Proceedings of 4th international conference on buildings and structures London, England. Cambridge: Cambridge University Press; 1975. p. 187–98.

[38] Matsuda K, Hikami Y, Fujiwara T, Moriyama A. Aerodynamic admittance and the 'strip theory' for horizontal buffeting forces on a bridge deck. J Wind Eng Indust Aerodynam 1999;83(13):337–46. http://dx.doi.org/10.1016/S0167-6105(99)00083-5.

[39] Xu Y, Xia Y. Structural health monitoring of long-span suspension bridges. Taylor & Francis; 2011. p. 39–74 [chapter 3].

[40] Steigen RO. Modeling and analyzing a suspension bridge in light of deterioration of the main cable wires Master's thesis. University of Stavanger; 2011.

[41] Bendat J, Piersol A. Random data: analysis and measurement procedures, Wiley series in probability and statistics. Wiley; 2011.

[42] Macdonald JH, Daniell WE. Variation of modal parameters of a cable-stayed bridge identified from ambient vibration measurements and fe modelling. Eng Struct 2005;27(13):1916–30. http://dx.doi.org/10.1016/j.engstruct.2005.06.007.

[43] Siringoringo DM, Fujino Y. System identification of suspension bridge from ambient vibration response. Eng Struct 2008;30(2):462–77. http://dx.doi.org/10.1016/j.engstruct.2007.03.004.

[44] Wang H, Wu T, Tao T, Li A, Kareem A. Measurements and analysis of non-stationary wind characteristics at sutong bridge in typhoon damrey. J Wind Eng Indust Aerodynam 2016;151:100–6. http://dx.doi.org/10.1016/j.jweia.2016.02.001.

[45] Holmes J. Wind loading of structures. CRC Press; 2007.

[46] Kaimal J, Wyngaard J, Izumi Y, Coté O. Spectral characteristics of surface-layer turbulence. Tech. rep., DTIC Document; 1972.

[47] Welch PD. The use of fast fourier transform for the estimation of power spectra: a method based on time averaging over short, modified periodograms. IEEE Trans Audio Electroacoust 1967;15:70–3.

[48] Carter G, Knapp C, Nuttall AH. Estimation of the magnitude-squared coherence function via overlapped fast fourier transform processing. IEEE Trans Audio Electroacoust 1973;21(4):337–44. http://dx.doi.org/10.1109/TAU.1973.1162496.

[49] Saranyasoontorn K, Manuel L, Veers PS. A comparison of standard coherence models for inflow turbulence with estimates from field measurements. J Solar Energy Eng 2004;126(4):1069–82. http://dx.doi.org/10.1115/1.1797978.

[50] Cheynet E, Bogunović Jakobsen J, Snæbjörnsson JT. Full scale monitoring of wind and traffic induced response of a suspension bridge. MATEC Web Conf 2015;24:04003. http://dx.doi.org/10.1051/matecconf/20152404003.

[51] Jain A, Jones NP, Scanlan RH. Coupled flutter and buffeting analysis of lon–span bridges. J Struct Eng 1996;122(7):716–25. http://dx.doi.org/10.1061/(ASCE)0733-9445(1996)122:7(716).

[52] Thorbek L, Hansen S. Coupled buffeting response of suspension bridges. J Wind Eng Indust Aerodynam 1998;7476:839–47. http://dx.doi.org/10.1016/S0167-6105(98)00076-2.

[53] Tveiten J. Dynamic analysis of a suspension bridge Master's thesis. University of Stavanger; 2012.

[54] Tanaka H, Davenport AG. Response of taut strip models to turbulent wind. J Eng Mech Div 1982;108(1):33–49.

[55] Zhu L, Xu Y, Zhang F, Xiang H. Tsing ma bridge deck under skew winds – Part i: Aerodynamic coefficients. J Wind Eng Indust Aerodynam 2002;90(7):781–805. http://dx.doi.org/10.1016/S0167-6105(02)00160-5.

[56] Diana G, Falco M, Bruni S, Cigada A, Larose G, Darnsgaard A, Collina A. Third asian-pacific symposium on wind engineering comparisons between wind tunnel tests on a full aeroelastic model of the proposed bridge over stretto di messina and numerical results. J Wind Eng Indust Aerodynam 1995;54:101–13. http://dx.doi.org/10.1016/0167-6105(94)00034-B.

[57] Zhu L, Wang M, Wang D, Guo Z, Cao F. Flutter and buffeting performances of third Nanjing Bridge over Yangtze River under yaw wind via aeroelastic model test. J Wind Eng Indust Aerodynam 2007;95(911):1579–606. http://dx.doi.org/

10.1016/j.jweia.2007.02.019. The fourth European and African conference on wind engineering.
[58] Xu Y, Sun D, Ko J, Lin J. Fully coupled buffeting analysis of tsing ma suspension bridge. J Wind Eng Indust Aerodynam 2000;85(1):97–117. http://dx.doi.org/10.1016/S0167-6105(99)00133-6.
[59] Kristensen L, Jensen NO. Lateral coherence in isotropic turbulence and in the natural wind. Bound-Layer Meteorol 1979;17(3):353–73. http://dx.doi.org/10.1007/BF00117924.
[60] Frandsen J. Simultaneous pressures and accelerations measured full-scale on the great belt east suspension bridge. J Wind Eng Indust Aerodynam 2001;89(1):95–129. http://dx.doi.org/10.1016/S0167-6105(00)00059-3.
[61] Chen J, Hui MCH, Xu YL. A comparative study of stationary and non-stationary wind models using field measurements. Bound-Layer Meteorol 2007;122(1):105–21. http://dx.doi.org/10.1007/s10546-006-9085-1.
[62] Hu L, Xu Y-L, Huang W-F. Typhoon-induced non-stationary buffeting response of long-span bridges in complex terrain. Eng Struct 2013;57:406–15. http://dx.doi.org/10.1016/j.engstruct.2013.09.044.
[63] Chen X, Kareem A. Advanced analysis of coupled buffeting response of bridges: a complex modal decomposition approach. Probabil Eng Mech 2002;17(2):201–13. http://dx.doi.org/10.1016/S0266-8920(02)00005-X.
[64] Øiseth O, Rönnquist A, Sigbjörnsson R. Effects of co-spectral densities of atmospheric turbulence on the dynamic response of cable-supported bridges: a case study. J Wind Eng Indust Aerodynam 2013;116:83–93. http://dx.doi.org/10.1016/j.jweia.2013.03.001.
[65] Denoël V. Application des méthodes d'analyse stochastique à l' étude des effets du vent sur les structures du génie civil Phd thesis. University of Liège; 2005.